

# Evaluation of the Invariant Reactions in the Ta-Rich Region of the Ta-B System

Vanessa Motta Chad, Érika Coaglia Trindade Ramos, Gilberto Carvalho Coelho, Carlos Angelo Nunes, Paulo Atsushi Suzuki, Flávio Ferreira, and Peter Rogl

(Submitted January 10, 2006; in revised form April 6, 2006)

Invariant reactions in the Ta-rich side of the Ta-B system were evaluated. The alloys were arc melted from pure materials. Pellets prepared from powder mixtures of Ta and TaB were heat treated under vacuum at 1900 and 1950 °C. The microstructures of the alloys were characterized through scanning electron microscopy images and x-ray diffraction (XRD). The microstructural analyses confirmed the type of reactions occurring in Ta-rich region; however, the composition of the liquid phase should be altered: (a)  $L \leftrightarrow Ta_{SS} + Ta_2B$  from 23 to 18 at.% B and (b)  $L + TaB \leftrightarrow Ta_2B$  from 27 to 22.5 at.% B. The formation of  $Ta_3B_2$  was confirmed as the understoichiometry of  $Ta_2B$ . The decomposition of  $Ta_2B$  occurs between 1900 and 1950 °C. The XRD data for alloys with composition between 34 and 50 at.% B indicate the existence of a new high-temperature phase.

**Keywords** borides, phase diagram, Ta-B system

## 1. Introduction

The authors have been evaluating the phase equilibria of RM-Si-B (RM: refractory metals) systems with potential for structural applications at high temperatures. Important discrepancies have been observed between their data and those of the literature for the RM-rich region of RM-B binaries.<sup>[1-3]</sup> During an experimental investigation in the Ta-rich corner of the Ta-Si-B system, discrepancies were observed between the currently accepted Ta-B phase diagram and the authors' results. This article reports their results concerning the invariant reactions in the Ta-rich region of the Ta-B system.

The currently accepted Ta-B phase diagram,<sup>[4]</sup> based on the studies of Leitnaker et al.,<sup>[5]</sup> Rudy and Windisch,<sup>[6]</sup> and Portnoi et al.,<sup>[7]</sup> is shown in Fig. 1. The reported solid phases in the 50 to 100% Ta region are TaB,  $Ta_3B_2$ ,  $Ta_2B$ , and  $Ta_{SS}$ . From previous investigations there is no doubt about the stability of these phases and the congruent formation of TaB. However, with respect to the  $Ta_2B$  phase, Nowotny et al.<sup>[8]</sup> suggest a peritectic formation through  $L + Ta_3B_2 \leftrightarrow Ta_2B$ , while Rudy and Windisch<sup>[6]</sup> and Portnoi et al.<sup>[7]</sup> report  $L + TaB \leftrightarrow Ta_2B$ . A contradiction also exists

concerning the phases involved in the peritectoid formation of  $Ta_3B_2$ : Leitnaker et al.<sup>[5]</sup> propose the reaction  $Ta_2B + TaB \leftrightarrow Ta_3B_2$ , while Portnoi et al.<sup>[7]</sup> suggest  $Ta_{SS} + TaB \leftrightarrow Ta_3B_2$ . Finally, it is interesting to notice that the  $Ta_2B$  occurs at understoichiometric composition, approximately 30 at.% B, as proposed by Leitnaker et al.<sup>[5]</sup> and accepted by Rudy and Windisch.<sup>[6]</sup>

## 2. Experimental Procedure

Ta-B alloys (~3 g) were produced by arc melting pure Ta (min 99.9%) and B (min 99.5%) under argon atmosphere (99.995%) in a water-cooled copper hearth, with a nonconsumable tungsten electrode and titanium getter. Five melting steps were carried out for each alloy to produce chemically homogeneous samples. Table 1 shows the composition of the alloys, the mass losses associated with the melting steps, and the calculated composition interval for each alloy assuming that all mass losses were either from Ta or B volatilization. The mass losses were less than 0.52%, which allows one to assume that near nominal compositions were kept.

To assess the stability of  $Ta_3B_2$ , pellets with 32 at.% B (68Ta-32B) were produced from pure Ta and TaB powder mixture (particle size < 177 μm) by cold pressing. They were heat treated under vacuum at 1900 and 1950 °C for 3 h, followed by furnace cooling. The temperatures were measured with a Type-C (W-Re) thermocouple placed close to the samples as well as with a calibrated infrared (IR) pyrometer.

The microstructures of the alloys were characterized through scanning electron microscopy/backscattered electron image (SEM/BSE) and x-ray diffraction (XRD). For the SEM analysis, the samples were hot mounted, ground with SiC paper (No. 120 to 4000), and then polished with colloidal silica suspension. The BSE images were obtained with acceleration voltage between 15 and 25 kV. The XRD experiments were performed at room temperature (Cu Kα

Vanessa Motta Chad, Érika Coaglia Trindade Ramos, Gilberto Carvalho Coelho, Carlos Angelo Nunes, and Paulo Atsushi Suzuki, FAENQUIL, Departamento de Engenharia de Materiais (DEMAR), Polo Urbo-Industrial Gleba AI-6, Caixa Postal 116, 12600-970, Lorena, SP, Brazil; Flávio Ferreira, UFF- Escola de Engenharia Industrial Metalúrgica de Volta Redonda—TMC, Avenida dos Trabalhadores 420, Vila Santa Cecília, 27255-125, Volta Redonda, RJ, Brazil; and Peter Rogl, Universität Wien, Institut für Physikalische Chemie, Währingerstrasse 42, A-1090 Wien, Austria. Contact e-mail: vanessa@phase.faelquil.br.

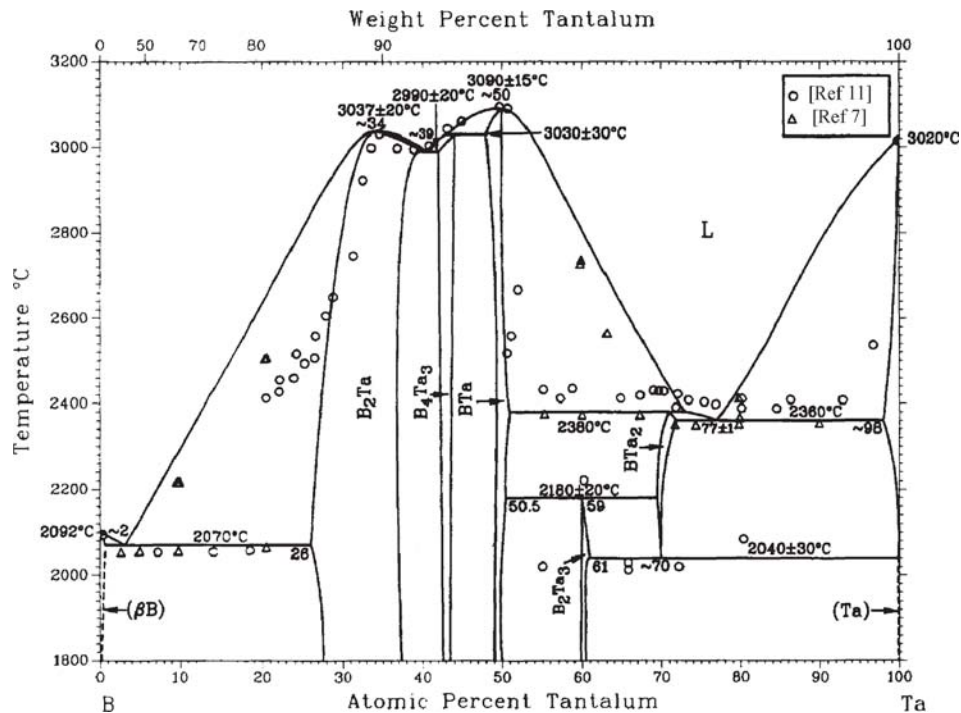


Fig. 1 Ta-B phase diagram. Source: Ref 4

Table 1 Compositions of the Ta-B alloys prepared in this work

Alloy No.	Composition, at.% B	Mass loss, %	Composition range, at.% B		Assumed composition, at.%
			(a)	(b)	
1	10	0.06	9.14	10.00	90Ta-10B
2	18	0.07	17.19	18.01	82Ta-18B
3	19	0.06	18.14	19.00	81Ta-19B
4	21	0.10	19.87	21.00	79Ta-21B
5	22	0.03	21.97	22.00	78Ta-22B
6	23	0.04	22.71	23.00	77Ta-23B
7	24	0.06	23.36	24.00	78Ta-24B
8	30	0.14	28.78	30.02	70Ta-30B
9	32	0.17	30.77	32.22	68Ta-32B
10	33	0.13	31.91	33.04	67Ta-33B
11	34	0.04	33.69	34.01	66Ta-34B
12	40	0.43	37.13	40.11	60Ta-40B
13	45	0.33	43.20	45.09	55Ta-45B
14	47	0.19	46.04	47.04	53Ta-47B
15	50	0.31	48.59	50.08	50Ta-50B

(a) Composition of the alloy considering mass loss attributed to tantalum volatilization. (b) Composition of the alloy considering mass loss attributed to boron volatilization

radiation) from powders (<177 μm) under the following conditions: 10° ≤ 2θ ≤ 90°, 0.05° step, and 2 s counting time. The XRD patterns were indexed using simulated diffraction patterns obtained from the PCW program<sup>[9]</sup> and crystallographic data from Villars and Calvert.<sup>[10]</sup>

### 3. Results and Discussion

The microstructure of the as-cast 90Ta-10B alloy indicates primary Ta<sub>SS</sub> dendrites and a eutectic structure in the interdendritic region constituted of Ta<sub>SS</sub> and Ta<sub>2</sub>B according to the SEM/BSE image (Fig. 2a) and XRD data (Fig. 3a). This is in agreement with Fig. 1 and confirms the existence of the L ↔ Ta<sub>SS</sub> + Ta<sub>2</sub>B eutectic reaction in this system.

The microstructure of the as-cast 82Ta-18B alloy presents a eutectic structure composed by Ta<sub>SS</sub> and Ta<sub>2</sub>B according to the SEM/BSE image (Fig. 2b) and XRD data (Fig. 3b), with no indication of primary phases. Based on Fig. 1 this alloy should have presented primary Ta<sub>SS</sub>. Thus, this result indicates that the liquid eutectic composition (L ↔ Ta<sub>SS</sub> + Ta<sub>2</sub>B) is located close to 18 at.% B and not at 23 at.% B as proposed in Fig. 1. It should be pointed out that the liquid eutectic composition at 18 at.% B is in agreement with the data from Nowotny et al.<sup>[8]</sup>

Primary precipitation of Ta<sub>2</sub>B and the Ta<sub>SS</sub> + Ta<sub>2</sub>B eutectic are observed in the microstructures of the as-cast 81Ta-19B, 79Ta-21B, and 78Ta-22B alloys according to the SEM/BSE images and XRD data. Figure 2(c) shows a SEM/BSE image of the 81Ta19B sample and Fig. 3(c) its diffractograms. The presence of primary Ta<sub>2</sub>B in this microstructure supports the proposition of the liquid eutectic composition near 18 at.% B as discussed previously.

The 77Ta-23B alloy presents an as-cast microstructure consisting of TaB, Ta<sub>2</sub>B, and Ta<sub>SS</sub> phases according to the SEM/BSE image (Fig. 2d) and XRD data (Fig. 3d). The Ta<sub>SS</sub> + Ta<sub>2</sub>B eutectic is noted in the last region to solidify. The primary precipitation of Ta<sub>2</sub>B in the 78Ta-22B alloy

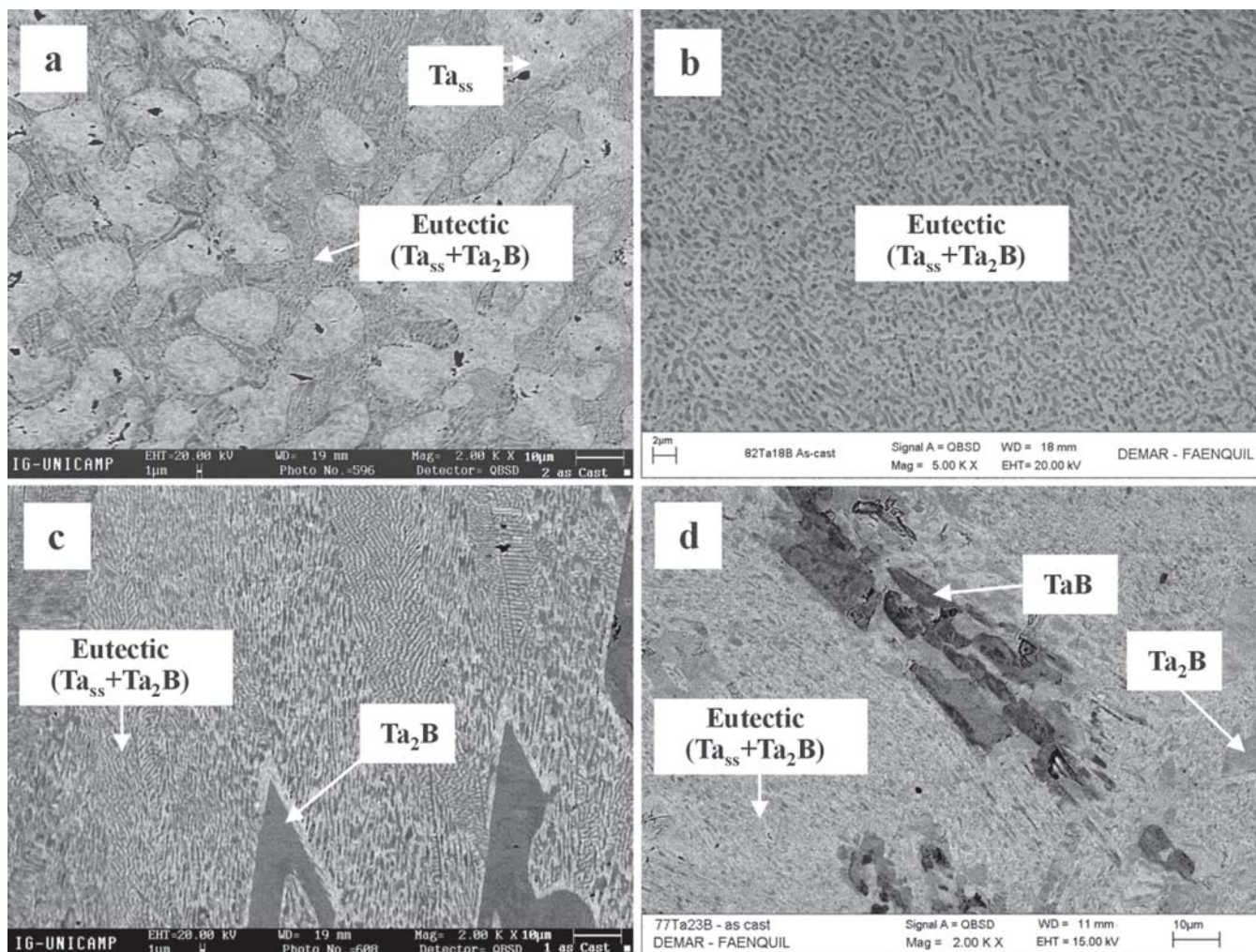


Fig. 2 SEM/BSE micrographs of as-cast (a) 90Ta-10B, (b) 82Ta-18B, (c) 81Ta-19B, and (d) 77Ta-23B alloys

and TaB in the 77Ta-23B alloy lead to the conclusion that the liquid peritectic composition corresponding to the reaction  $L + \text{TaB} \leftrightarrow \text{Ta}_2\text{B}$  is placed between 22 and 23 at.% B. This result does not agree with Fig. 1, which proposes a liquid composition of approximately 27 at.% B for this reaction. However, it confirms the peritectic formation of  $\text{Ta}_2\text{B}$  as proposed by Rudy and Windisch<sup>[6]</sup> and Portnoi et al.<sup>[7]</sup>

The as-cast alloys with composition between 23 and 50 at.% B present TaB,  $\text{Ta}_2\text{B}$ , and  $\text{Ta}_{\text{SS}}$  phases in their microstructure according to the SEM/BSE images and XRD data. However, for boron compositions higher than 34 at.%, at least two important XRD peaks are observed in the diffractograms that could not be attributed to any of the stable solid phases of the Ta-B system (particularly  $\text{Ta}_3\text{B}_2$ ). Figures 3(e) and (f) show the diffractograms of the 66Ta-34B and 55Ta-45B alloys, respectively, where the unknown peaks are found. No special contrast was observed in the SEM/BSE images, giving no hints to understanding the phase transformation taking place. At this point, the authors attribute this finding to a possible polymorphic transformation of either TaB or  $\text{Ta}_2\text{B}$  during cooling, a result that has not

yet been reported in literature. Considering that these peaks are not observed in the 49Ta-51B alloy, which is essentially formed by TaB, it is more likely that the new phase is a  $\text{Ta}_2\text{B}$  polymorph. A tentative attempt to increase the amount of the new phase was done by heat treating the as-cast alloys with B compositions higher than 34 at.% at 1900 and 1950 °C. All the extra peaks were not observed in the diffractograms of the heat treated alloys, suggesting that this new phase is stable only at higher temperatures. Further work has to be carried out to identify and characterize this new phase.

The experiments carried out to evaluate the stability of  $\text{Ta}_3\text{B}_2$  and the temperature of the  $\text{Ta}_2\text{B} \leftrightarrow \text{Ta}_{\text{SS}} + \text{Ta}_3\text{B}_2$  invariant gave these results: after heat treatment of the Ta + TaB (32 at.% B) pellet at 1900 °C, only  $\text{Ta}_{\text{SS}} + \text{Ta}_3\text{B}_2$  were present. On the other hand, after heat treatment of pellets with the same composition at 1950 °C, a mixture of  $\text{Ta}_3\text{B}_2$  and  $\text{Ta}_2\text{B}$  was observed. Therefore, the eutectoid decomposition of  $\text{Ta}_2\text{B}$  is located between 1900 and 1950 °C, in opposition to  $2040 \pm 30$  °C proposed by Leitnaker et al.<sup>[5]</sup> In addition, these results also confirm the understoichiometry of  $\text{Ta}_2\text{B}$  at approximately 30 at.% B.<sup>[5,6]</sup>

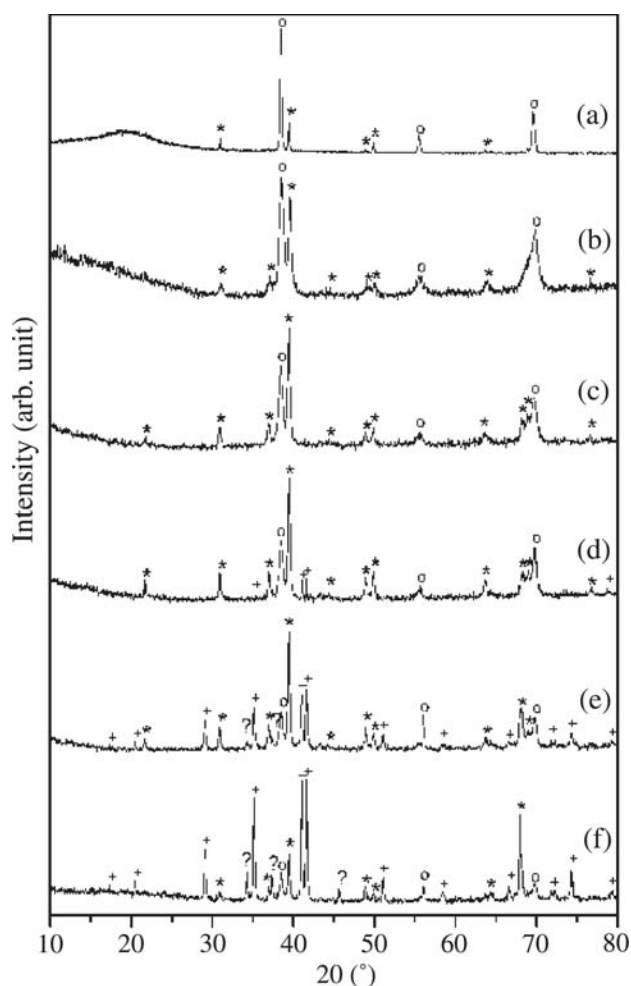


**Fig. 3** X-ray diffractograms of as-cast (a) 90Ta-10B, (b) 82Ta-18B, (c) 81Ta-19B, (d) 77Ta-23B, (e) 66Ta-34B, and (f) 55Ta-45B alloys. ○, Ta<sub>SS</sub>; \*, Ta<sub>2</sub>B; +, TaB; ?, unknown phase

#### 4. Conclusions

In this work, the authors evaluated the invariant reactions in the Ta-rich side of the Ta-B system. Carefully conducted microstructural analyses of several alloys in the 50 to 100% Ta range confirmed the type of reactions occurring in that

region. However, the composition of the liquid phase should be altered: (a)  $L \leftrightarrow \text{Ta}_{\text{SS}} + \text{Ta}_2\text{B}$  from 23 at.% B to 18 at.% B and (b)  $L + \text{TaB} \leftrightarrow \text{Ta}_2\text{B}$  from 27 to 22.5 at.% B. The formation of Ta<sub>3</sub>B<sub>2</sub> through solid-state reaction was confirmed, occurring between 1900 and 1950 °C, as well as the understoichiometry of Ta<sub>2</sub>B. The XRD data for alloys with composition between 34 and 50 at.% B indicate the existence of a new high-temperature phase not yet reported in the literature.

#### Acknowledgment

The authors acknowledge FAPESP (São Paulo, Brazil) for financial support under grant No. 00/11620-0.

#### References

1. L.A. Borges Jr., G.C. Coelho, C.A. Nunes, and P.A. Suzuki, New Data on Phase Equilibria in the Nb-Rich Region of the Nb-B System, *J. Phase Equilibria*, 2003, **24**(2), p 140-146
2. B.B. Lima, C.A. Nunes, G.C. Coelho, P.A. Suzuki, and P. Rogl, Evaluation of the Invariant Reactions of the V-B System, *J. Phase Equilibria Diffus.*, 2004, **25**(2), p 134-139
3. C.A. Nunes, D. Kaczorowski, P. Rogl, M.R. Balgissera, P.A. Suzuki, G.C. Coelho, A. Grytsiv, G. André, F. Bouréé, and S. Okada, The NbB<sub>2</sub>-Phase Revisited: Homogeneity Range, Defect Structure, Superconductivity, *Acta Mater.*, 2005, **53**, p 3679-3687
4. H. Okamoto, Comment on Boron-Tantalum, *J. Phase Equilibria*, 1993, **14**(3), p 393-394
5. J.M. Leitnaker, M.G. Bowman, and P.W. Gilles, High-Temperature Phase Studies in the Tantalum-Boron System between Ta and TaB, *J. Electrochem. Soc.*, 1961, **108**(6), p 568-572
6. E. Rudy and S.T. Windisch, Technical Report AFML-TR-65-2, Part I, Vol X, Wright-Patterson Air Force Base, OH, 1966
7. K.I. Portnoi, V.M. Romashov, and S.E. Salibekov, Constitution Diagram of the System Tantalum-Boron, *Sov. Powder Metall. Met. Ceram.*, 1971, **10**(11), p 925-927
8. H. Nowotny, F. Benesovsky, and R. Kieffer, Beitrag zum Aufbau der Systeme Niob-Bor und Tantal-Bor, *Z. Metallkd.*, 1959, **50**(7), p 417-423
9. W. Kraus and G. Nolze, POWDERCELL—A Program for the Representation and Manipulation of Crystal Structures and Calculation of the Resulting X-Ray Powder Patterns, *J. Appl. Crystallogr.*, 1996, **29**, p 301-303
10. P. Villars and L.D. Calvert, *Pearson's Handbook of Crystallographic Data for Intermetallic Phases*, 2nd ed., ASM International, 1991